

1  
2  
3  
4  
5  
6  
7  
8  
9  
10  
11  
12  
13  
14  
15  
16  
17  
18  
19  
20  
21  
22  
23  
24  
25  
26  
27  
28  
29  
30  
31  
32  
33  
34

## Metaphloem development in the Arabidopsis root tip

Moritz Graeff and Christian S. Hardtke\*

Department of Plant Molecular Biology, University of Lausanne, Biophore Building, 1015  
Lausanne, Switzerland

\* Corresponding author: [christian.hardtke@unil.ch](mailto:christian.hardtke@unil.ch)

**Keywords:** Arabidopsis, root, protophloem, metaphloem, sieve element, OPS

**Summary statement:** Metaphloem sieve element differentiation in Arabidopsis roots follows a robust developmental trajectory.

35 **ABSTRACT**

36 The phloem transport network is a major evolutionary innovation that enabled plants to dominate  
37 terrestrial ecosystems. In the growth apices, the meristems, apical stem cells continuously  
38 produce early, so-called protophloem. This is easily observed in Arabidopsis root meristems,  
39 where the differentiation of individual protophloem sieve element precursors into interconnected,  
40 conducting sieve tubes is laid out in a spatio-temporal gradient. The mature protophloem  
41 eventually collapses as the neighboring metaphloem takes over its function further distal from the  
42 stem cell niche. Compared to protophloem, metaphloem ontogenesis is poorly characterized,  
43 primarily because its visualization is challenging. Here we describe an improved protocol to  
44 investigate metaphloem development in Arabidopsis root tips in combination with a set of new  
45 molecular markers. We found that mature metaphloem sieve elements are only observed in the  
46 late post-meristematic root although their specification is initiated as soon as protophloem sieve  
47 elements enucleate. Moreover, unlike protophloem sieve elements, metaphloem sieve elements  
48 only differentiate once they have fully elongated. Finally, our results suggest that metaphloem  
49 differentiation is not directly controlled by protophloem-derived cues but rather follows a distinct,  
50 robust developmental trajectory.

51

## 52 INTRODUCTION

53 The evolution of vascular tissues enabled plants to conquer land because it allowed the  
54 separation of the sites of photosynthesis from the sites of nutrient and water acquisition (Lucas et  
55 al., 2013). In extant angiosperms, the xylem vessels form hollow tubes to transport water and  
56 inorganic ions from the root system to the shoot system. This transport is mainly driven by the  
57 water potential differential between the soil and the atmosphere, and therefore by purely physical  
58 forces (Endo et al., 2019; Pratt and Jacobsen, 2017). Closely associated with the xylem is the  
59 phloem, which is composed of inter-connected sieve elements that form the conducting sieve  
60 tubes and their neighboring companion cells. Unlike xylem vessels, sieve elements are not dead,  
61 but during their differentiation process, they drastically alter their cellular makeup to optimize the  
62 transport flow. Most noticeable, they lose their nucleus and vacuole. Thus, sieve elements depend  
63 on the neighboring companion cells for the maintenance of their transport functions. Phloem sieve  
64 tubes mediate the long distance bulk transport of phloem sap, a viscous mix of sugars,  
65 metabolites as well as systemic signaling molecules, from source to sink organs, for example  
66 from mature photosynthesizing leaves to roots (Lopez-Salmeron et al., 2019). This transport is  
67 driven by a differential in osmotic pressure, which builds up through the controlled loading of  
68 osmotic sugars in the source tissue phloem and their unloading in the sink tissue phloem  
69 (Knoblauch et al., 2016; Zhang and Turgeon, 2018). The growth apices of plants, the meristems,  
70 are terminal sinks, whose activity is sustained by phloem sap delivered through the early, so-  
71 called protophloem. In root meristems, protophloem is produced by apical stem cells that reside  
72 adjacent to the quiescent center (QC) and matures while neighboring tissues still divide or  
73 undergo expansion growth (Esau, 1977; Lopez-Salmeron et al., 2019). Eventually, its sieve  
74 elements become non-functional and are completely obliterated as protophloem is replaced by  
75 emerging metaphloem. Although the metaphloem sieve elements share a common precursor with  
76 protophloem sieve elements (Bonke et al., 2003; Rodriguez-Villalon et al., 2014), the metaphloem  
77 only matures after the expansion growth of the surrounding tissues is completed (Esau, 1977).  
78 Metaphloem is then retained as the main conducting phloem, although it can later be replaced by  
79 secondary phloem in species that undergo secondary growth.

80 Non-invasive investigation of phloem development is challenging, on the one hand  
81 because sieve elements are thin and highly anisotropic cells, and on the other hand because the  
82 phloem is buried deep inside plant organs. Routine observation of protophloem by confocal  
83 microscopy is however possible in the root tip of *Arabidopsis thaliana* (Arabidopsis), where its  
84 development is laid out in a spatio-temporal gradient of ~20 cells from stem cell daughter to  
85 mature sieve element (Furuta et al., 2014; Rodriguez-Villalon et al., 2014). Arabidopsis root tips

86 produce two protophloem strands, which are arranged opposite each other inside the stele,  
87 flanking an axis of xylem cells (Fig. 1A). The last two decades have seen tremendous advances  
88 in our understanding of protophloem ontogeny. Through its dissection by genetic approaches,  
89 numerous protophloem-specific mutants and molecular markers have become available. These  
90 studies underline the essential character of root protophloem, whose absence or disturbed  
91 development has grave, systemic consequences on root meristem growth and maintenance  
92 (Anne and Hardtke, 2017; Bonke et al., 2003; Rodriguez-Villalon et al., 2014). Whether the  
93 defects in the protophloem of pertinent mutants also extend to metaphloem remains largely  
94 unknown, mainly because of the difficulty in visualizing metaphloem development and a paucity  
95 of specific molecular markers for non-invasive investigation. Here we set out to mend this gap by  
96 developing a toolbox for the analysis of metaphloem development.

97

## 98 **RESULTS AND DISCUSSION**

### 99 **An optimized protocol for metaphloem visualization by confocal microscopy**

100 Imaging of the Arabidopsis root tip by confocal microscopy techniques is routine but can be tricky  
101 depending on the tissue targeted for investigation. In particular, this applies to the cells inside the  
102 stele, which are small in diameter compared to the surrounding ground tissue or epidermis (Fig.  
103 1A). For instance, whereas the diameter of cortex cells reaches ~25 to ~50 micrometers,  
104 protophloem cells are a mere ~5 micrometers across and therefore roughly 20 times smaller in  
105 their horizontal cross section profile (Fig. 1A). Together, the vascular tissues inside the stele  
106 occupy merely ~10% of the area in a root meristem cross section, although they represent ~40%  
107 of cell files. Despite progress in staining and fixation techniques, visualization of these cells can  
108 sometimes be challenging. For instance, while developing protophloem sieve elements (PPSEs)  
109 can be readily identified because of their early differentiation and associated cell wall build up  
110 (Truernit, 2014), mature, enucleated PPSEs are difficult to observe. Initially, PPSEs elongate from  
111 the ~20 micrometer typical of dividing cells to an intermediate stage of ~50 micrometer during  
112 which the principal differentiation steps occur. Once they are enucleated, they still elongate rapidly  
113 to about twice their length as they become the conductive unloading terminus of the PPSE cell  
114 file (Ross-Elliott et al., 2017). It is likely their high anisotropy in combination with a still elongating,  
115 soft cell wall that is responsible for the compression of maturing PPSEs by neighboring tissues  
116 once they lose their elevated turgor during fixation. Elongating cells possess relatively soft primary  
117 cell walls to facilitate directional expansion. Stabilizing secondary cell walls are only deposited  
118 during the final stages of differentiation, when the cells have reached their final size and adapt to  
119 their future roles. The phenomenon of cell shrinkage or collapse upon fixation is generally  
120 observed once all tissues have started to elongate further distal, in the generic cell elongation  
121 zone of the root meristem (Fig. S1A). The developing metaphloem sieve elements (MPSEs) are  
122 thus particularly affected, rendering their observation difficult with existing standard protocols, like  
123 chloral hydrate clearing (McBryde, 1936) or mPS-PI staining (Truernit et al., 2008). By contrast,  
124 the recently developed ClearSee (Kurihara et al., 2015) and TDE (2'2-thiodiethanol) clearing  
125 (Musielak et al., 2016) protocols not only preserved the structure of this delicate area (Fig. S1B)  
126 but also the fluorescence of reporter proteins.

127 Starting from these recent advances, we sought to develop a protocol that would leave  
128 the elongation area intact and permit routine observation of MPSEs. Through a test series with  
129 various combinations and concentrations of described detergents, clearing agents and fixation  
130 steps (Kurihara et al., 2015; Musielak et al., 2016; Ursache et al., 2018), we established an  
131 optimized procedure that maintained the integrity of the root elongation zone and allowed us to

132 observe the progressive development of MPSE cell files (the “TetSee” protocol, see Materials and  
133 Methods) (Fig. S1C). Starting from the second formative division in the phloem lineage, the  
134 division that gives rise to the PPSE and MPSE cell files (Bonke et al., 2003; Rodriguez-Villalon et  
135 al., 2014), we could follow MPSE files across overlapping 3D renderings of serial confocal  
136 microscopy images (Fig. 1B). The morphologically visible onset of MPSE differentiation, as judged  
137 by intensified calcofluor white cell wall staining, was on average observed as far as ~1,400  
138 micrometers from the QC. This was substantially later than the onset of morphological  
139 differentiation of PPSEs (~120 micrometer from the QC), trichoblasts (~620 micrometer from the  
140 QC) or protoxylem (~680 micrometer from the QC) (Fig. 1C). Thus, MPSEs only differentiated  
141 visibly once all other tissues had already matured, with the exception of the metaxylem, which  
142 differentiated around the same time or slightly later.

### 143 **Metaphloem sieve elements differentiate after they have reached their final cell size**

144 Interestingly, whereas cell elongation and differentiation are tightly linked in PPSEs (Furuta et al.,  
145 2014; Rodriguez-Villalon et al., 2014), MPSEs elongated to roughly their final size before any cell  
146 wall build up became apparent (Fig. 1B). Observation of other cellular rearrangements indicative  
147 of MPSE differentiation, notably enucleation, proved to be difficult because of the high anisotropy  
148 of MPSEs and against the background from neighboring tissues, for example when nucleic acid  
149 dyes such as DAPI were used. However, our morphology-based observations were corroborated  
150 by analyses of a generic molecular marker of cellular differentiation in Arabidopsis, the MINIYO  
151 (IYO) protein (Sanmartin et al., 2011). Constitutively expressed IYO-GFP fusion protein is barely  
152 visible in the cytosol but accumulates in the nucleus once cells differentiate. In the root tip, IYO-  
153 GFP was therefore clearly visible in the quickly differentiating distal root tissues, the columella  
154 and lateral root cap (Fig. 2A). Among the proximal root tissues, protophloem is the first to  
155 differentiate and consistently, nuclear IYO-GFP accumulation became first apparent in  
156 differentiating PPSEs (Fig. 2A) (Sanmartin et al., 2011). Interestingly, they were followed by their  
157 companion cells with some distance, suggesting that PPSE companion cells only differentiate  
158 once PPSEs are fully elongated and functional (Fig. 2A). In the stele, developing protoxylem  
159 displayed nuclear IYO-GFP next (Fig. 2B), followed with some delay by MPSE cell files (Fig. 2C).  
160 In fact, nuclear IYO-GFP accumulation was only observed in developing MPSEs after developing  
161 protoxylem vessels had already completed their secondary wall build up and after they had  
162 themselves fully elongated (Fig. 2D). In summary, both our morphological and molecular analyses  
163 suggest that unlike in PPSEs, cell elongation and terminal differentiation do not coincide in  
164 MPSEs.

## 165 **A set of new molecular markers for the investigation of metaphloem development**

166 Although nuclear IYO accumulation is a very useful generic indicator of the onset of cellular  
167 differentiation (Sanmartin et al., 2011), it is not a marker for cell specification. We therefore sought  
168 to identify tissue-specific molecular markers that would allow us to trace the incipient beginnings  
169 of MPSE development. To this end, we mined the literature for genes that are specifically  
170 expressed in mature phloem in other contexts (Anstead et al., 2012; Bonke et al., 2003; Cayla et  
171 al., 2015; Khan et al., 2007; Sankar et al., 2014) and chose seven genes for further investigation.  
172 Moreover, we intersected existing phloem-related gene expression data sets (Brady et al., 2007;  
173 Clark et al., 2019; Kondo et al., 2016; Zhao et al., 2005) to identify a set of 14 additional  
174 metaphloem marker candidates. For some of them, existing reporter plasmids could be obtained,  
175 but for the majority we cloned promoter constructs that drive the expression of a nuclear localized  
176 fluorescent reporter (NLS-CITRINE). After their transformation into Col-0 wildtype plants, eight  
177 out of the 21 reporters showed activity in developing root phloem: the described *SISTER OF*  
178 *ALTERED PHLOEM DEVELOPMENT* (*SAPL*) (Ross-Elliott et al., 2017), *EARLY NODULIN-LIKE*  
179 *9* (*ENODL9*) (Khan et al., 2007), *SIEVE ELEMENT OCCLUSION-RELATED 2* (*SEOR2*) (Anstead  
180 et al., 2012) and *SECONDARY WALL-ASSOCIATED NAC DOMAIN PROTEIN 2* (*SND2*) (Kim et  
181 al., 2020) reporters (Fig. 3A-D); and the new reporters *DESIGUAL 2* (*DEAL2*) (Wilson-Sanchez  
182 et al., 2018), *SIEVE ELEMENT MARKER 1* (*SEMA1*; AT2G35585), *SEMA2* (AT1G61760) and  
183 *SEMA3* (AT3G26350) (Fig. 4A-D).

184 However, none of the reporters was exclusively active in the (incipient) metaphloem,  
185 rather, all markers were also expressed in the late developing protophloem. Among them, the  
186 *SAPL* expression was particular, because although it was expressed in late differentiating PPSEs  
187 similar to the other markers, thereafter it was highly specific for companion cells, both in the proto-  
188 and metaphloem, and not detected in developing MPSEs (Fig. 3A). Notably, *SAPL* was  
189 continuously expressed from the early coincidence with PPSE differentiation onward beyond  
190 differentiated MPSEs and was not observed in any other cell file. This suggests that the four  
191 companion cell files subsequently serve both PPSE and MPSE maintenance. The other markers  
192 were expressed in PPSEs as well as MPSEs, with varying levels of specificity. All of them were  
193 expressed in developing PPSEs, after the onset of cell wall build up and coincident with the partial  
194 elongation that occurs before enucleation. *ENODL9*, *SEOR2* and *SEMA1* were most specific for  
195 developing sieve elements (Figs. 3C,D and 4B). However, whereas *SEOR2* and *SEMA1*  
196 expression gradually ceased upon PPSE differentiation and only became active again later,  
197 *ENODL9* expression switched to the incipient MPSE file earlier and stayed on until MPSE  
198 differentiation terminated (Fig. 3D). Moreover, *SEOR2* expression reappeared earlier than

199 *SEMA1* expression (Figs. 3C and 4B). The other reporters also displayed some marked  
200 expression outside of PPSEs/MPSEs. The *SND2* reporter was strongly expressed in late  
201 developing MPSEs, however it was also observed in developing metaxylem (Fig. 3B). *DEAL2*,  
202 *SEMA2* and *SEMA3* all switched expression to the cell files surrounding PPSEs after enucleation  
203 (Fig. 4A,C,D). In the metaphloem, *DEAL2* was expressed in MPSEs but also in the directly  
204 neighboring cell files, likely the companion cells (Fig. 4A). A similar pattern was observed for  
205 *SEMA3* (Fig. 4D), whereas *SEMA2* appeared to be specific for MPSEs (Fig. 4C). In summary, we  
206 were able to identify a set of reporters for metaphloem development that mark different stages as  
207 well as cell types (Fig. 4E). Their investigation confirmed that unlike what has been reported for  
208 PPSEs, cell elongation and differentiation are uncoupled in MPSEs, and also show that both sieve  
209 element types are associated with the same companion cell files.

### 210 **Metaphloem development is not affected by CLE45 treatment**

211 The continuous expression of *ENODL9* in the MPSE cell files as soon as PPSEs enucleate also  
212 suggested that MPSE specification starts as soon as PPSE development is finished. This could  
213 mean that premature MPSE differentiation is prevented by lateral inhibition through cues derived  
214 from developing PPSEs. One such candidate signal are secreted CLAVATA3/EMBRYO  
215 SURROUNDING REGION-RELATED (CLE) signaling peptides, because low concentrations of  
216 certain synthetic CLE peptides suppress PPSE development when applied to roots (Depuydt et  
217 al., 2013; Hazak et al., 2017; Ito et al., 2006; Kinoshita et al., 2007; Rodriguez-Villalon et al.,  
218 2014), as does dosage increase of CLE45 (Czyzewicz et al., 2015b; Rodriguez-Villalon et al.,  
219 2014). Interestingly, CLE45 as well as CLE26 and CLE25 are specifically expressed in developing  
220 PPSEs (Czyzewicz et al., 2015a; Ren et al., 2019; Rodriguez-Villalon et al., 2014; Rodriguez-  
221 Villalon et al., 2015). CLE peptide signaling is however apparently not strictly required for  
222 protophloem development (Anne et al., 2018; Fukuda and Hardtke, 2020), rather it appears to act  
223 as a safeguard mechanism that maintains plasticity of phloem pole cells during their meristematic  
224 stage (Gujas et al., 2020).

225 Upon CLE45 treatment, the expression of both markers tested, *SEMA3* and *SEOR2*,  
226 disappeared from the protophloem, consistent with their prohibitive effect on PPSE formation (Fig.  
227 5A-D). However, both markers persisted in developing MPSEs (Fig. 5B,D), in line with the  
228 observation that their differentiation appeared unaffected. Notably, this observation also  
229 confirmed once more that MPSE specification is position- rather than lineage-dependent, because  
230 the PPSE and MPSE cell files arise from the same stem cell daughter through a periclinal division  
231 that is suppressed by CLE45 application (Rodriguez-Villalon et al., 2014; Rodriguez-Villalon et  
232 al., 2015). Moreover, the absence of pertinent phenotypes in *cle25* mutants (Ren et al., 2019) as



233 well as in receptor mutants that are fully insensitive against all three CLE peptides (Anne et al.,  
234 2018) corroborates the conclusion that PPSE-derived CLE peptides do not impinge on MPSE  
235 development under normal circumstances. In summary, CLE45 peptide treatment efficiently  
236 suppressed PPSE formation, but did not interfere with MPSE development.

### 237 **MPSE development follows a robust developmental trajectory**

238 In the protophloem, CLE45 signaling is quantitatively antagonized by the vascular plant -specific  
239 *OCTOPUS* (*OPS*) gene. *OPS* is thus a positive regulator of PPSE differentiation that is expressed  
240 from early on in the protophloem and insulates developing PPSEs against the effects of autocrine  
241 CLE45 signalling (Breda et al., 2017; Breda et al., 2019). In *ops* loss-of-function mutants,  
242 developing PPSEs frequently fail to differentiate (including failure to build up cell wall and thereby  
243 appearing as so-called gap cells), which causes discontinuities in the protophloem strands and  
244 disturbs the transport of phloem sap into the meristem (Anne and Hardtke, 2017; Rodriguez-  
245 Villalon et al., 2014; Truernit et al., 2012). *OPS* is also weakly expressed in the incipient MPSE  
246 cell file, against a background of low, ubiquitous expression of its homolog *OPS-LIKE 2* (*OPL2*)  
247 that increases in developing metaphloem (Ruiz Sola et al., 2017). Whereas *opl2* single mutants  
248 did not display apparent phenotypes, except (in our hands) a more variable root growth vigor (Fig.  
249 S2A), the *ops opl2* double mutant is the only described genotype with MPSE defects so far (Fig.  
250 S2B) (Ruiz Sola et al., 2017), apart from mutants that lack protophloem and metaphloem  
251 altogether. Compared to *ops* single mutants, root growth vigor was further diminished in *ops opl2*  
252 double mutants (Fig. S2A,C) and they also displayed aggravated PPSE differentiation defects  
253 (Fig. S2B,D) (Ruiz Sola et al., 2017). The latter were more severe than evident from simple gap  
254 cell presence-absence counts, because *ops opl2* double mutants often had only one  
255 distinguishable PPSE strand. To better understand how MPSE and PPSE differentiation is  
256 affected in *ops* single and *ops opl2* double mutants, we introduced some of our reporter genes  
257 into these backgrounds.

258 In *ops* single mutants, the *SEMA3* reporter was expressed at the later stages of PPSE  
259 differentiation as in wildtype, but absent in developing PPSEs that failed to differentiate (Fig. S3A),  
260 underlining their different cellular identity. In developing MPSEs, *SEMA3* expression appeared to  
261 be unaffected (Fig. S3B,C). By contrast, *SAPL* reporter activity was still observed in gap cells  
262 (Fig. S3D), which corroborates earlier observations and is in line with the recent proposal that  
263 they adopt companion cell identity (Gujas et al., 2020) as well as the strong continuous companion  
264 cell-specific *SAPL* expression after PPSE differentiation. Again, *SAPL* expression appeared  
265 unaffected in the developing metaphloem region of *ops* mutants (Fig. S3E). Together, these  
266 findings reiterate that the defects in *ops* mutants are protophloem-specific (Ruiz Sola et al., 2017;

267 Truernit et al., 2012). Interestingly, *SAPL* expression could still be detected in protophloem gap  
268 cells later on (Fig. S3F), indicating that PPSE cells that fail to differentiate properly in the  
269 protophloem differentiation window fail to catch up.

270 In *ops ops* double mutants, the *SEOR2*, *DEAL2*, *SEMA2* and *SEMA3* markers displayed  
271 normal expression, except their apparent absence in gap cells (Fig. 6A-D). Despite the described  
272 MPSE differentiation defects (Ruiz Sola et al., 2017), which we could also observe in optical cross  
273 sections (Fig. S2B), our markers were however essentially continuously expressed in developing  
274 MPSEs of *ops ops* mutants (Fig. 6A-D). Thus, we could not detect corresponding “metaphloem  
275 gap cells”, possibly because differentiating MPSEs are quite long (200-300 micrometer) and  
276 because surveying extended stretches of MPSEs was difficult. Nevertheless, although *ops ops*  
277 double mutants typically displayed marker expression in both PPSE and MPSE strands (Fig. 7A),  
278 this pattern also often deviated from wildtype. Upon closer inspection, this could be attributed to  
279 the reappearance of reporter expression in undifferentiated protophloem cell files long after the  
280 zone of normal PPSE differentiation, clearly visible from elongated PPSEs that expressed the  
281 respective marker (Fig. 7B). Thus, the observation that one of the two protophloem poles in *ops*  
282 *ops* mutants was frequently absent (Fig. S2B) (Ruiz Sola et al., 2017) could also reflect a strongly  
283 delayed differentiation of one PPSE strand. *In extremis*, the delay was such that it overlapped  
284 with reporter expression in the neighboring MPSE cell files (Fig. 7C). We had not observed such  
285 atypical differentiation in *ops* single mutants. This not only indicates that PPSE differentiation can  
286 be substantially delayed in *ops ops* mutants, but also that the onset of MPSE differentiation is  
287 largely independent of such delays. Corroborating the independent trajectory of MPSE  
288 differentiation, in *ops ops* roots where only one PPSE cell file showed differentiating cells (any  
289 gap cells notwithstanding) and marker expression was also absent from the failed PPSE cell file  
290 later on, marker expression in both MPSE cell files appeared to be normal (Fig. 7D) and could  
291 typically be observed shortly after protoxylem cells with secondary cell walls were visible, as in  
292 wildtype. Together with the observed activity of our markers in CLE45-treated roots, our analyses  
293 therefore suggest that MPSE development follows a robust trajectory that is largely independent  
294 from PPSE development.

295 Finally, it is noteworthy that OPS action is exquisitely dosage-sensitive (Breda et al., 2017;  
296 Breda et al., 2019) and promotes PPSE differentiation by quantitatively antagonizing CLE45  
297 signaling via the receptor kinase BARELY ANY MERISTEM 3 (Breda et al., 2017; Breda et al.,  
298 2019; Fukuda and Hardtke, 2020). Moreover, an excess of ectopic OPS activity leads to  
299 premature differentiation across root tissues (Breda et al., 2019). Thus, our results are consistent  
300 with the notion that the differential expression levels of OPS family proteins such as *OPS* and

301 *OPL2* along the gradient of developing PPSE versus MPSE cell files contributes to the correct  
302 spatio-temporal separation of their differentiation.

### 303 **A toolbox for the investigation of metaphloem development**

304 In summary, our study extends our toolbox for the investigation of sieve element development in  
305 the *Arabidopsis* root, with a special focus on the so far poorly described differentiation of the  
306 metaphloem, and provides first forays into its genetic control. Our results highlight commonalities  
307 between PPSE and MPSE development, but also suggest that metaphloem development follows  
308 a robust trajectory that is not directly influenced by adjacent or preceding PPSE development  
309 under normal circumstances. Combined with state-of-the-art technical advances, such as single  
310 cell RNA sequencing or tissue-specific gene knock-out (Smetana et al., 2019; Wendrich et al.,  
311 2020), our observations should enable more targeted future approaches to dissect metaphloem  
312 development and discover its unique features.

313

## 314 MATERIALS AND METHODS

315 Plant culture, transformation and common molecular biology followed previously described  
316 standard procedures (Cattaneo et al., 2019; Graeff et al., 2020; Kang et al., 2017).

### 317 Plant materials and growth conditions

318 Seeds were surface sterilized using 3% sodium hypochlorite, sown onto half strength Murashige  
319 & Skoog agar medium (0.9% agarose) supplemented with 0.3% sucrose and stratified for 3 days  
320 at 4°C. Plants were grown under continuous white light (intensity ~120 µE) at 22°C. All mutants  
321 and marker lines were in the *Arabidopsis thaliana* Columbia-0 (Col-0) wild type background. The  
322 *ops* and *ops opl2* mutant lines were described previously (Ruiz Sola et al., 2017; Truernit et al.,  
323 2012). CLE45 peptide treatments were performed as described (Anne et al., 2018).

### 324 Database mining and selection of sieve element marker candidates

325 For the selection of the sieve element (SE) marker candidates, expression of 576 genes enriched  
326 in cells expressing the S32 phloem marker (AT2G18380) was analysed along the root, in cells  
327 expressing *SUC2* (AT1G22710) (Brady et al., 2007), in cells expressing *CVP2* (AT1G05470)  
328 (Clark et al., 2019), in a general root and seedling gene expression dataset (Gan et al., 2011),  
329 and in the “VISUAL” phloem and xylem datasets (Kondo et al., 2016). Twenty candidate genes  
330 that i) showed expression in the phloem poles, ii) showed increased expression further away from  
331 the meristem, iii) showed relatively higher expression in the root, and iv) appeared in the VISUAL  
332 phloem datasets were tested as SE markers.

### 333 Transgene constructs

334 For the construction of SE markers, respective promoter fragments of 1,500 bp to 2,500 bp were  
335 amplified from genomic Col-0 DNA using suitable oligonucleotides with overhangs (attB1/2  
336 extensions for *ENODL9*, *SEOR2*, *SND2*, and attB4/1r extensions for *DEAL2* and *SEMA1-3*) for  
337 subsequent *Gateway*<sup>TM</sup> cloning (see Table S1). The manufacturer’s solutions (*ThermoFisher*  
338 *Scientific* article numbers 11791020 and 11789020) and protocols were used for all cloning  
339 reactions. Amplified fragments were cloned into suitable entry vectors and the *ENODL9*, *SEOR2*  
340 and *SND2* promoters were transferred into the pMDC205 destination vector in front of a GFP  
341 reporter with an ER retention signal (Curtis and Grossniklaus, 2003). The *DEAL2* and *SEMA1-3*  
342 promoters were recombined together with NLS-CITRINE in a multisite gateway reaction into the  
343 pK7m24 vector backbone. Flowering Col-0 plants were transformed using the floral dip method  
344 and transformants were selected either on ½ MS media containing 25 mg/ml hygromycin B or 25  
345 mg/ml kanamycin following a fast selection procedure (Harrison et al., 2006).

### 346 **Tissue fixation and clearing (TetSee protocol)**

347 For microscopy, 7-day-old seedlings were fixed in a solution of 4% PFA in PBS buffer and  
348 transferred into a vacuum of 25 to 30 mmHg/Torr for 15 to 30 min. Subsequently, seedlings were  
349 washed three times in PBS for 5 min. For clearing of the samples, different protocols were used  
350 and assessed for the quality of the tissue preservation along the root. While standard protocols  
351 like chloral hydrate clearing (McBryde, 1936) or mPS-PI staining (Truernit et al., 2008) caused  
352 the shrinking of the cells in the early elongation zone, the recently developed ClearSee (Kurihara  
353 et al., 2015) and 2'2-thiodiethanol-clearing (Musielak et al., 2016) protocols preserved the  
354 structure of this delicate area as well as the fluorescence of reporter proteins. The two protocols  
355 were further optimized and combined into the “TetSee” (2'2-Thiodiethanol-ClearSee) protocol.  
356 Briefly, the washed seedlings were transferred into TetSee X solution (15% Na-deoxycholate,  
357 25% urea, 10 % glycerol, 5% 2'2-thiodiethanol [Merck, Product No. 166782], 1% Triton X-100)  
358 and kept for 3 days at 4°C with daily changes of the TetSee X solution. For microscopy, the  
359 TetSee X solution was removed and replaced by TetSee solution (the TetSee X solution without  
360 Triton X-100) containing 0.25 mg/ml calcofluor white (CCFW; Sigma, Product No. F3543).  
361 Seedlings were incubated in the CCFW staining solution for 6 h or overnight, washed once in  
362 TetSee solution and then transferred onto microscopy slides with TetSee solution as mounting  
363 medium.

### 364 **Microscopy**

365 For morphological assessment of phloem differentiation, roots were prepared as described above  
366 and the CCFW-stained cell walls were imaged using a Zeiss LSM880 confocal microscope with  
367 a 40x objective. A 405 nm laser was used for CCFW excitation, and the cell wall signal was  
368 recorded in a range from 450 to 480 nm. For imaging of the SE marker lines, GFP or CITRINE  
369 were sequentially excited with 488 nm and their emission recorded from 500 to 560 nm. Tile scans  
370 and Z scans were combined in order to obtain continuous images of the vasculature from the root  
371 meristem to the differentiated metaphloem. Additionally, a Nikon Spinning disc CSU-W1 confocal  
372 microscope with a 40x objective was used to record images of the CLE45-treated and the *ops*  
373 *opl2* SE marker lines. Analysis of the images and generation of 3D renderings from the Z stacks  
374 were performed using the *GNU icy* software.

375

376 **ACKNOWLEDGEMENTS**

377 We would like to thank Dr. Y. Helariutta for a gift of the *pSAPL::erGFP* reporter plasmid, and Drs.  
378 J. Sanchez-Serrano and E. Rojo for a gift of the *p35S::IYO-GFP* plasmid and transgenic line.

379 **COMPETING INTERESTS**

380 The authors declare no competing interests.

381 **FUNDING**

382 This work was funded by Swiss National Science Foundation grant 310030B\_185379 (awarded  
383 to C.S.H.) and the Deutsche Forschungsgemeinschaft post-doctoral fellowship GR 5009/1-1  
384 (awarded to M.G.).  
385

386 **FIGURE LEGENDS**

387 **Fig. 1. Development of metaphloem sieve elements (MPSEs) in the Arabidopsis root tip.**

388 (A) Schematic overview of tissue arrangement and development in an Arabidopsis root meristem,  
389 based on confocal microscopy images of a longitudinal half section and a horizontal cross section.  
390 (B) Confocal microscopy, optical sections illustrating MPSE development in a 7-day-old  
391 Arabidopsis Col-0 wildtype root tip stained with calcofluor white (CCFW; blue fluorescence) and  
392 propidium iodide (PI; reddish fluorescence) using the optimized “TetSee” protocol. Left overview  
393 panels indicate the approximate positions of the magnified images in the right panels. The bottom  
394 right panels are labeled counterparts of the raw images in the corresponding top right panels. The  
395 common stem cell precursors for the protophloem sieve element (PPSE) and MPSE cell files are  
396 labeled in red in the left-most assembly. Note the formative division giving rise to the developing  
397 PPSE strand (labeled green) and incipient MPSE strand (labeled yellow). Size bars are 10  
398 micrometer. (C) Distance of the first visibly differentiated cell from the quiescent center, for  
399 different root tissues. Box plots display 2nd and 3rd quartiles and the median, bars indicate  
400 maximum and minimum.

401 **Fig. 2. Differentiation timing in the Arabidopsis root tip.** (A-D) 3D renderings of confocal

402 image stacks, focused on the vasculature. Consecutive sections of a 7-day-old CCFW-stained  
403 root expressing the IYO-GFP fusion protein (green fluorescence) under control of the constitutive  
404 35S promoter are shown. Left panels: CCFW-GFP fluorescence composite images; right panels:  
405 GFP fluorescence only. Nuclear IYO-GFP accumulation indicates cellular differentiation.  
406 Differentiating PPSEs are pointed out by a red arrowhead, their companion cells by white  
407 arrowheads (A). Protoxylem cells (blue arrowheads) start to differentiate before MPSEs (orange  
408 arrowheads) (B), who enter differentiation once secondary wall build up in protoxylem cells  
409 becomes apparent (C,D).

410 **Fig. 3. Reporter genes for phloem specification and differentiation I.** (A-D) 3D renderings of

411 confocal image stacks, focused on the vasculature of 7-day-old CCFW-stained roots that express  
412 the indicated reporter genes (green fluorescence). Left overview panels (generic wildtype root)  
413 indicate the approximate positions of the magnified images in the right panels. Bottom panels:  
414 CCFW-GFP fluorescence composite images; top panels: GFP fluorescence only. Note that for  
415 better visibility of details, images are not always to the same scale.

416 **Fig. 4. Reporter genes for phloem specification and differentiation II.** (A-D) 3D renderings of

417 confocal image stacks, focused on the vasculature of 7-day-old CCFW-stained roots that express  
418 the indicated reporter genes (green fluorescence). Left overview panels (generic wildtype root)

419 indicate the approximate positions of the magnified images in the right panels. Bottom panels:  
420 CCFW-GFP fluorescence composite images; top panels: GFP fluorescence only. (E) Schematic  
421 summary of the tissue-specific expression patterns for the reporter genes shown in figures 3 and  
422 4.

423 **Fig. 5. MPSE reporter genes do not respond to CLE45-treatment.** (A-D) 3D renderings of  
424 confocal image stacks, focused on the vasculature of 7-day-old CCFW-stained roots that express  
425 the indicated reporter genes (green fluorescence). Left overview panels (generic wildtype root,  
426 treated with mock or CLE45) indicate the approximate positions of the magnified images in the  
427 right panels. Bottom panels: CCFW-GFP fluorescence composite images; top panels: GFP  
428 fluorescence only. Roots were either grown on mock (A,C) or 15 nM CLE45 peptide (B,D).

429 **Fig. 6. Phloem reporter gene expression in *ops opl2* double mutants I.** (A-D) 3D renderings  
430 of confocal image stacks, focused on the vasculature of 7-day-old CCFW-stained roots that  
431 express the indicated reporter genes (green fluorescence) in *ops opl2* double mutant background.  
432 Left overview panels (generic *ops opl2* root) indicate the approximate positions of the magnified  
433 images in the right panels. Center panels: CCFW-GFP fluorescence composite images; right  
434 panels: GFP fluorescence only. Note that for better viewing of details, images are not always to  
435 the same scale.

436 **Fig. 7. Phloem reporter gene expression in *ops opl2* double mutants II.** (A-D) 3D renderings  
437 of confocal image stacks, focused on the vasculature of 7-day-old CCFW-stained roots that  
438 express the indicated reporter genes (green fluorescence) in *ops opl2* double mutant background.  
439 Left panels: CCFW-GFP fluorescence composite images; right panels: GFP fluorescence only.  
440 PPSE or MPSE cell files expressing molecular markers are pointed out by red or orange  
441 arrowheads, respectively.

442



443 **SUPPLEMENTARY FIGURE LEGENDS**

444 **Fig. S1. Imaging of elongating root cells using different fixation protocols.** (A-C) Confocal  
445 microscopy, optical sections of 7-day-old CCFW-stained root meristems (white fluorescence)  
446 fixed with different protocols as indicated. Red arrowheads point out elongating PPSEs.

447 **Fig. S2. Root phenotypes of *ops op12* double mutants.** (A) Primary root length of 12-day-old  
448 seedlings of indicated genotypes. Box plots display 2nd and 3rd quartiles and the median, bars  
449 indicate maximum and minimum. (B) Confocal microscopy, longitudinal and horizontal optical  
450 cross sections of 7-day-old CCFW-stained root meristems (black fluorescence). Full red  
451 arrowheads point out normally differentiating PPSEs, open red arrowheads point out cells in the  
452 PPSE file that fail to differentiate ("gap cells). (C) Images of 12-day-old seedlings of the indicated  
453 genotypes. (D) Frequency of PPSE cell files with gap cells in root meristems of the indicated  
454 genotypes (n=20-30).

455 **Fig. S3. Phloem reporter gene expression in *ops* single mutants.** (A-F) 3D renderings of  
456 confocal image stacks, focused on the vasculature of 7-day-old CCFW-stained roots that express  
457 the indicated reporter genes (green fluorescence) in *ops* single mutant background. Left overview  
458 panels (generic *ops* root) indicate the approximate positions of the magnified images in the right  
459 panels. Center panels: CCFW-GFP fluorescence composite images; top panels: GFP  
460 fluorescence only. Note that for better viewing of details, images are not always to the same scale.  
461 Open arrowheads in (A), (D) and (F) point out cells in the PPSE file that fail to differentiate ("gap  
462 cells).

463

464 REFERENCES

- 465 **Anne, P., Amiguet-Vercher, A., Brandt, B., Kalmbach, L., Geldner, N., Hothorn, M. and**  
466 **Hardtke, C. S.** (2018). CLERK is a novel receptor kinase required for sensing of root-  
467 active CLE peptides in Arabidopsis. *Development* **145**.
- 468 **Anne, P. and Hardtke, C. S.** (2017). Phloem function and development-biophysics meets  
469 genetics. *Curr Opin Plant Biol* **43**, 22-28.
- 470 **Anstead, J. A., Froelich, D. R., Knoblauch, M. and Thompson, G. A.** (2012). Arabidopsis P-  
471 protein filament formation requires both AtSEOR1 and AtSEOR2. *Plant Cell Physiol* **53**,  
472 1033-1042.
- 473 **Bonke, M., Thitamadee, S., Mahonen, A. P., Hauser, M. T. and Helariutta, Y.** (2003). APL  
474 regulates vascular tissue identity in Arabidopsis. *Nature* **426**, 181-186.
- 475 **Brady, S. M., Orlando, D. A., Lee, J. Y., Wang, J. Y., Koch, J., Dinneny, J. R., Mace, D., Ohler,**  
476 **U. and Benfey, P. N.** (2007). A high-resolution root spatiotemporal map reveals dominant  
477 expression patterns. *Science* **318**, 801-806.
- 478 **Breda, A. S., Hazak, O. and Hardtke, C. S.** (2017). Phosphosite charge rather than shootward  
479 localization determines OCTOPUS activity in root protophloem. *Proc Natl Acad Sci U S A*  
480 **114**, E5721-E5730.
- 481 **Breda, A. S., Hazak, O., Schultz, P., Anne, P., Graeff, M., Simon, R. and Hardtke, C. S.** (2019).  
482 A Cellular Insulator against CLE45 Peptide Signaling. *Current biology : CB* **29**, 2501-2508  
483 e2503.
- 484 **Cattaneo, P., Graeff, M., Marhava, P. and Hardtke, C. S.** (2019). Conditional effects of the  
485 epigenetic regulator JUMONJI 14 in Arabidopsis root growth. *Development* **146**.
- 486 **Cayla, T., Batailler, B., Le Hir, R., Revers, F., Anstead, J. A., Thompson, G. A., Grandjean,**  
487 **O. and Dinant, S.** (2015). Live imaging of companion cells and sieve elements in  
488 Arabidopsis leaves. *PloS one* **10**, e0118122.
- 489 **Clark, N. M., Buckner, E., Fisher, A. P., Nelson, E. C., Nguyen, T. T., Simmons, A. R., de Luis**  
490 **Balaguer, M. A., Butler-Smith, T., Sheldon, P. J., Bergmann, D. C., et al.** (2019). Stem-  
491 cell-ubiquitous genes spatiotemporally coordinate division through regulation of stem-cell-  
492 specific gene networks. *Nature communications* **10**, 5574.
- 493 **Curtis, M. D. and Grossniklaus, U.** (2003). A gateway cloning vector set for high-throughput  
494 functional analysis of genes in planta. *Plant Physiol* **133**, 462-469.
- 495 **Czyzewicz, N., Shi, C. L., Vu, L. D., Van De Cotte, B., Hodgman, C., Butenko, M. A. and De**  
496 **Smet, I.** (2015a). Modulation of Arabidopsis and monocot root architecture by  
497 CLAVATA3/EMBRYO SURROUNDING REGION 26 peptide. *J Exp Bot* **66**, 5229-5243.
- 498 **Czyzewicz, N., Wildhagen, M., Cattaneo, P., Stahl, Y., Pinto, K. G., Aalen, R. B., Butenko, M.**  
499 **A., Simon, R., Hardtke, C. S. and De Smet, I.** (2015b). Antagonistic peptide technology  
500 for functional dissection of CLE peptides revisited. *J Exp Bot* **66**, 5367-5374.
- 501 **Depuydt, S., Rodriguez-Villalon, A., Santuari, L., Wyser-Rmili, C., Ragni, L. and Hardtke, C.**  
502 **S.** (2013). Suppression of Arabidopsis protophloem differentiation and root meristem  
503 growth by CLE45 requires the receptor-like kinase BAM3. *Proc Natl Acad Sci U S A* **110**,  
504 7074-7079.
- 505 **Endo, S., Iwai, Y. and Fukuda, H.** (2019). Cargo-dependent and cell wall-associated xylem  
506 transport in Arabidopsis. *New Phytol* **222**, 159-170.
- 507 **Esau, K.** (1977). *Anatomy of seed plants* (2d edn). New York: Wiley.
- 508 **Fukuda, H. and Hardtke, C. S.** (2020). Peptide Signaling Pathways in Vascular Differentiation.  
509 *Plant Physiol* **182**, 1636-1644.
- 510 **Furuta, K. M., Yadav, S. R., Lehesranta, S., Belevich, I., Miyashima, S., Heo, J. O., Vaten, A.,**  
511 **Lindgren, O., De Rybel, B., Van Isterdael, G., et al.** (2014). Plant development.  
512 Arabidopsis NAC45/86 direct sieve element morphogenesis culminating in enucleation.  
513 *Science* **345**, 933-937.

- 514 **Gan, X., Stegle, O., Behr, J., Steffen, J. G., Drewe, P., Hildebrand, K. L., Lyngsoe, R.,**  
515 **Schultheiss, S. J., Osborne, E. J., Sreedharan, V. T., et al. (2011).** Multiple reference  
516 genomes and transcriptomes for *Arabidopsis thaliana*. *Nature* **477**, 419-423.
- 517 **Graeff, M., Rana, S., Marhava, P., Moret, B. and Hardtke, C. S. (2020).** Local and Systemic  
518 Effects of Brassinosteroid Perception in Developing Phloem. *Current biology : CB* **30**,  
519 1626-1638 e1623.
- 520 **Gujas, B., Kastanaki, E., Sturchler, A., Cruz, T. M. D., Ruiz-Sola, M. A., Dreos, R., Eicke, S.,**  
521 **Truernit, E. and Rodriguez-Villalon, A. (2020).** A Reservoir of Pluripotent Phloem Cells  
522 Safeguards the Linear Developmental Trajectory of Protophloem Sieve Elements. *Current*  
523 *biology : CB* **30**, 755-766 e754.
- 524 **Harrison, S. J., Mott, E. K., Parsley, K., Aspinall, S., Gray, J. C. and Cottage, A. (2006).** A  
525 rapid and robust method of identifying transformed *Arabidopsis thaliana* seedlings  
526 following floral dip transformation. *Plant Methods* **2**, 19.
- 527 **Hazak, O., Brandt, B., Cattaneo, P., Santiago, J., Rodriguez-Villalon, A., Hothorn, M. and**  
528 **Hardtke, C. S. (2017).** Perception of root-active CLE peptides requires CORYNE function  
529 in the phloem vasculature. *EMBO Rep* **18**, 1367-1381.
- 530 **Ito, Y., Nakanomyo, I., Motose, H., Iwamoto, K., Sawa, S., Dohmae, N. and Fukuda, H. (2006).**  
531 Dodeca-CLE peptides as suppressors of plant stem cell differentiation. *Science* **313**, 842-  
532 845.
- 533 **Kang, Y. H., Breda, A. and Hardtke, C. S. (2017).** Brassinosteroid signaling directs formative  
534 cell divisions and protophloem differentiation in *Arabidopsis* root meristems. *Development*  
535 **144**, 272-280.
- 536 **Khan, J. A., Wang, Q., Sjolund, R. D., Schulz, A. and Thompson, G. A. (2007).** An early  
537 nodulin-like protein accumulates in the sieve element plasma membrane of *Arabidopsis*.  
538 *Plant Physiol* **143**, 1576-1589.
- 539 **Kim, H., Zhou, J., Kumar, D., Jang, G., Ryu, K. H., Sebastian, J., Miyashima, S., Helariutta,**  
540 **Y. and Lee, J. Y. (2020).** SHORTROOT-Mediated Intercellular Signals Coordinate  
541 Phloem Development in *Arabidopsis* Roots. *Plant Cell* **32**, 1519-1535.
- 542 **Kinoshita, A., Nakamura, Y., Sasaki, E., Kyojuka, J., Fukuda, H. and Sawa, S. (2007).** Gain-  
543 of-function phenotypes of chemically synthetic CLAVATA3/ESR-related (CLE) peptides in  
544 *Arabidopsis thaliana* and *Oryza sativa*. *Plant Cell Physiol* **48**, 1821-1825.
- 545 **Knoblauch, M., Knoblauch, J., Mullendore, D. L., Savage, J. A., Babst, B. A., Beecher, S. D.,**  
546 **Dodgen, A. C., Jensen, K. H. and Holbrook, N. M. (2016).** Testing the Munch hypothesis  
547 of long distance phloem transport in plants. *Elife* **5**.
- 548 **Kondo, Y., Nurani, A. M., Saito, C., Ichihashi, Y., Saito, M., Yamazaki, K., Mitsuda, N., Ohme-**  
549 **Takagi, M. and Fukuda, H. (2016).** Vascular Cell Induction Culture System Using  
550 *Arabidopsis* Leaves (VISUAL) Reveals the Sequential Differentiation of Sieve Element-  
551 Like Cells. *Plant Cell* **28**, 1250-1262.
- 552 **Kurihara, D., Mizuta, Y., Sato, Y. and Higashiyama, T. (2015).** ClearSee: a rapid optical clearing  
553 reagent for whole-plant fluorescence imaging. *Development* **142**, 4168-4179.
- 554 **Lopez-Salmeron, V., Cho, H., Tonn, N. and Greb, T. (2019).** The Phloem as a Mediator of Plant  
555 Growth Plasticity. *Current biology : CB* **29**, R173-R181.
- 556 **Lucas, W. J., Groover, A., Lichtenberger, R., Furuta, K., Yadav, S. R., Helariutta, Y., He, X.**  
557 **Q., Fukuda, H., Kang, J., Brady, S. M., et al. (2013).** The plant vascular system:  
558 evolution, development and functions. *Journal of integrative plant biology* **55**, 294-388.
- 559 **McBryde, M. C. (1936).** A method of demonstrating rust hyphae and haustoria in unsectioned  
560 leaf tissue. *Am J Bot* **23**, 686-689.
- 561 **Musielak, T. J., Slane, D., Liebig, C. and Bayer, M. (2016).** A Versatile Optical Clearing Protocol  
562 for Deep Tissue Imaging of Fluorescent Proteins in *Arabidopsis thaliana*. *PloS one* **11**,  
563 e0161107.

- 564 **Pratt, R. B. and Jacobsen, A. L.** (2017). Conflicting demands on angiosperm xylem: Tradeoffs  
565 among storage, transport and biomechanics. *Plant Cell Environ* **40**, 897-913.
- 566 **Ren, S. C., Song, X. F., Chen, W. Q., Lu, R., Lucas, W. J. and Liu, C. M.** (2019). CLE25 peptide  
567 regulates phloem initiation in Arabidopsis through a CLERK-CLV2 receptor complex.  
568 *Journal of integrative plant biology*.
- 569 **Rodriguez-Villalon, A., Gujas, B., Kang, Y. H., Breda, A. S., Cattaneo, P., Depuydt, S. and**  
570 **Hardtke, C. S.** (2014). Molecular genetic framework for protophloem formation. *Proc Natl*  
571 *Acad Sci U S A* **111**, 11551-11556.
- 572 **Rodriguez-Villalon, A., Gujas, B., van Wijk, R., Munnik, T. and Hardtke, C. S.** (2015). Primary  
573 root protophloem differentiation requires balanced phosphatidylinositol-4,5-biphosphate  
574 levels and systemically affects root branching. *Development* **142**, 1437-1446.
- 575 **Ross-Elliott, T. J., Jensen, K. H., Haaning, K. S., Wager, B. M., Knoblauch, J., Howell, A. H.,**  
576 **Mullendore, D. L., Monteith, A. G., Paultre, D., Yan, D., et al.** (2017). Phloem unloading  
577 in Arabidopsis roots is convective and regulated by the phloem-pole pericycle. *Elife* **6**.
- 578 **Ruiz Sola, M. A., Coiro, M., Crivelli, S., Zeeman, S. C., Schmidt Kjolner Hansen, S. and**  
579 **Truernit, E.** (2017). OCTOPUS-LIKE 2, a novel player in Arabidopsis root and vascular  
580 development, reveals a key role for OCTOPUS family genes in root metaphloem sieve  
581 tube differentiation. *New Phytol* **216**, 1191-1204.
- 582 **Sankar, M., Nieminen, K., Ragni, L., Xenarios, I. and Hardtke, C. S.** (2014). Automated  
583 quantitative histology reveals vascular morphodynamics during Arabidopsis hypocotyl  
584 secondary growth. *Elife* **3**, e01567.
- 585 **Sanmartin, M., Sauer, M., Munoz, A., Zouhar, J., Ordonez, A., van de Ven, W. T., Caro, E.,**  
586 **de la Paz Sanchez, M., Raikhel, N. V., Gutierrez, C., et al.** (2011). A molecular switch  
587 for initiating cell differentiation in Arabidopsis. *Current biology : CB* **21**, 999-1008.
- 588 **Smetana, O., Makila, R., Lyu, M., Amiryousefi, A., Sanchez Rodriguez, F., Wu, M. F., Sole-**  
589 **Gil, A., Leal Gavarron, M., Siligato, R., Miyashima, S., et al.** (2019). High levels of auxin  
590 signalling define the stem-cell organizer of the vascular cambium. *Nature* **565**, 485-489.
- 591 **Truernit, E.** (2014). Phloem imaging. *J Exp Bot* **65**, 1681-1688.
- 592 **Truernit, E., Bauby, H., Belcram, K., Barthelemy, J. and Palauqui, J. C.** (2012). OCTOPUS,  
593 a polarly localised membrane-associated protein, regulates phloem differentiation entry in  
594 Arabidopsis thaliana. *Development* **139**, 1306-1315.
- 595 **Truernit, E., Bauby, H., Dubreucq, B., Grandjean, O., Runions, J., Barthelemy, J. and**  
596 **Palauqui, J. C.** (2008). High-resolution whole-mount imaging of three-dimensional tissue  
597 organization and gene expression enables the study of Phloem development and structure  
598 in Arabidopsis. *Plant Cell* **20**, 1494-1503.
- 599 **Ursache, R., Andersen, T. G., Marhavy, P. and Geldner, N.** (2018). A protocol for combining  
600 fluorescent proteins with histological stains for diverse cell wall components. *Plant J* **93**,  
601 399-412.
- 602 **Wendrich, J. R., Yang, B., Vandamme, N., Verstaen, K., Smet, W., Van de Velde, C., Minne,**  
603 **M., Wybouw, B., Mor, E., Arents, H. E., et al.** (2020). Vascular transcription factors guide  
604 plant epidermal responses to limiting phosphate conditions. *Science*.
- 605 **Wilson-Sanchez, D., Martinez-Lopez, S., Navarro-Cartagena, S., Jover-Gil, S. and Micol, J.**  
606 **L.** (2018). Members of the DEAL subfamily of the DUF1218 gene family are required for  
607 bilateral symmetry but not for dorsoventrality in Arabidopsis leaves. *New Phytol* **217**, 1307-  
608 1321.
- 609 **Zhang, C. and Turgeon, R.** (2018). Mechanisms of phloem loading. *Curr Opin Plant Biol* **43**, 71-  
610 75.
- 611 **Zhao, C., Craig, J. C., Petzold, H. E., Dickerman, A. W. and Beers, E. P.** (2005). The xylem  
612 and phloem transcriptomes from secondary tissues of the Arabidopsis root-hypocotyl.  
613 *Plant Physiol* **138**, 803-818.
- 614

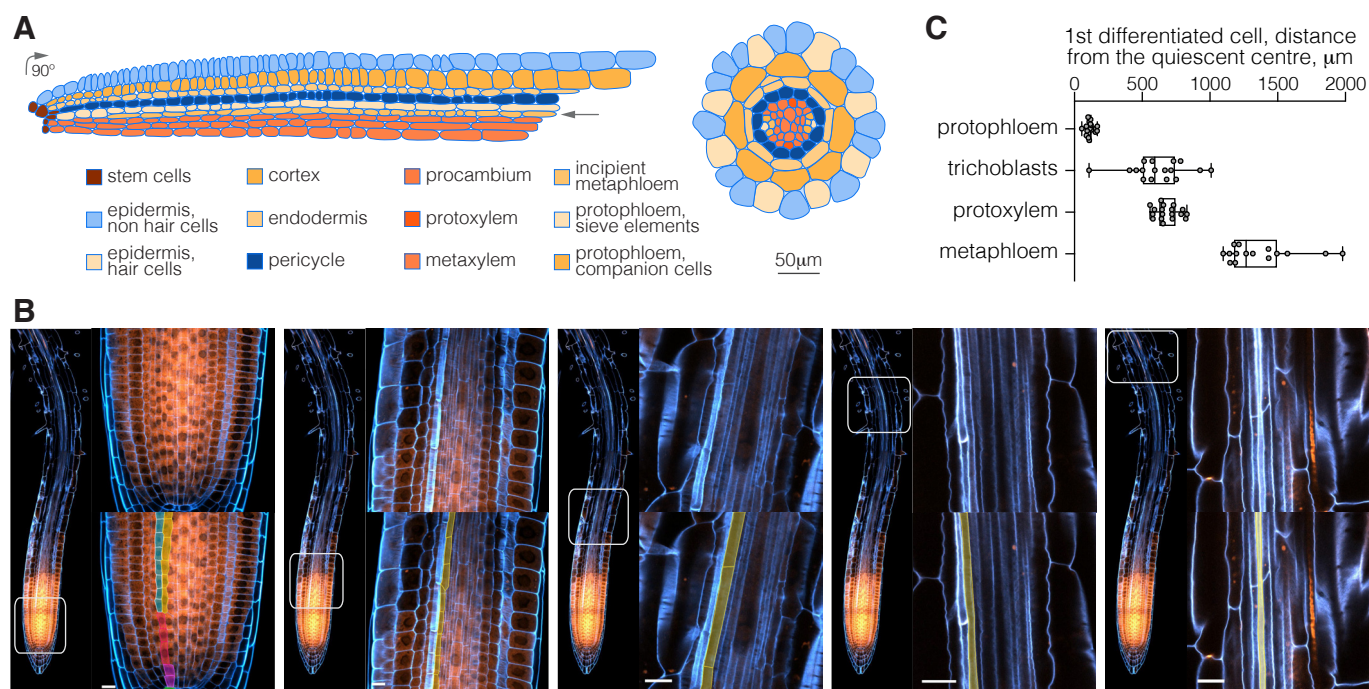


**Fig. 1. Development of metaphloem sieve elements (MPSEs) in the Arabidopsis root tip.** (A) Schematic overview of tissue arrangement and development in an Arabidopsis root meristem, based on confocal microscopy images of a longitudinal half section and a horizontal cross section. (B) Confocal microscopy, optical sections illustrating MPSE development in a 7-day-old Arabidopsis Col-0 wildtype root tip stained with calcofluor white (CCFW; blue fluorescence) and propidium iodide (PI; reddish fluorescence) using the optimized "TetSee" protocol. Left overview panels indicate the approximate positions of the magnified images in the right panels. The bottom right panels are labeled counterparts of the raw images in the corresponding top right panels. The common stem cell precursors for the protophloem sieve element (PPSE) and MPSE cell files are labeled in red in the left-most assembly. Note the formative division giving rise to the developing PPSE strand (labeled green) and incipient MPSE strand (labeled yellow). Size bars are 10 micrometer. (C) Distance of the first visibly differentiated cell from the quiescent center, for different root tissues. Box plots display 2nd and 3rd quartiles and the median, bars indicate maximum and minimum.

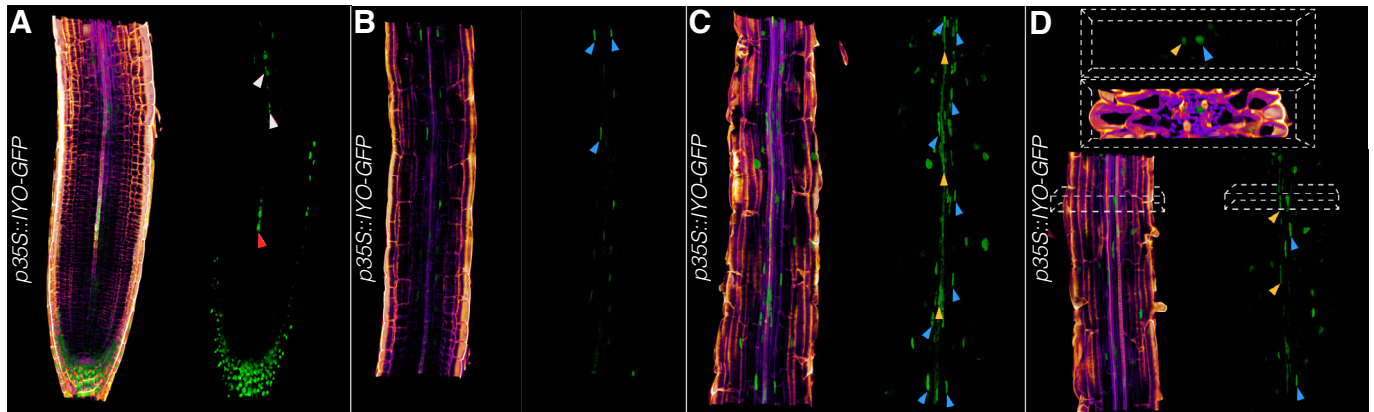


**Fig. 2. Differentiation timing in the Arabidopsis root tip.** (A-D) 3D renderings of confocal image stacks, focused on the vasculature. Consecutive sections of a 7-day-old CCFW-stained root expressing the IYO-GFP fusion protein (green fluorescence) under control of the constitutive 35S promoter are shown. Left panels: CCFW-GFP fluorescence composite images; right panels: GFP fluorescence only. Nuclear IYO-GFP accumulation indicates cellular differentiation. Differentiating PPSEs are pointed out by a red arrowhead, their companion cells by white arrowheads (A). Protoxylem cells (blue arrowheads) start to differentiate before MPSEs (orange arrowheads) (B), who enter differentiation once secondary wall build up in protoxylem cells becomes apparent (C,D).

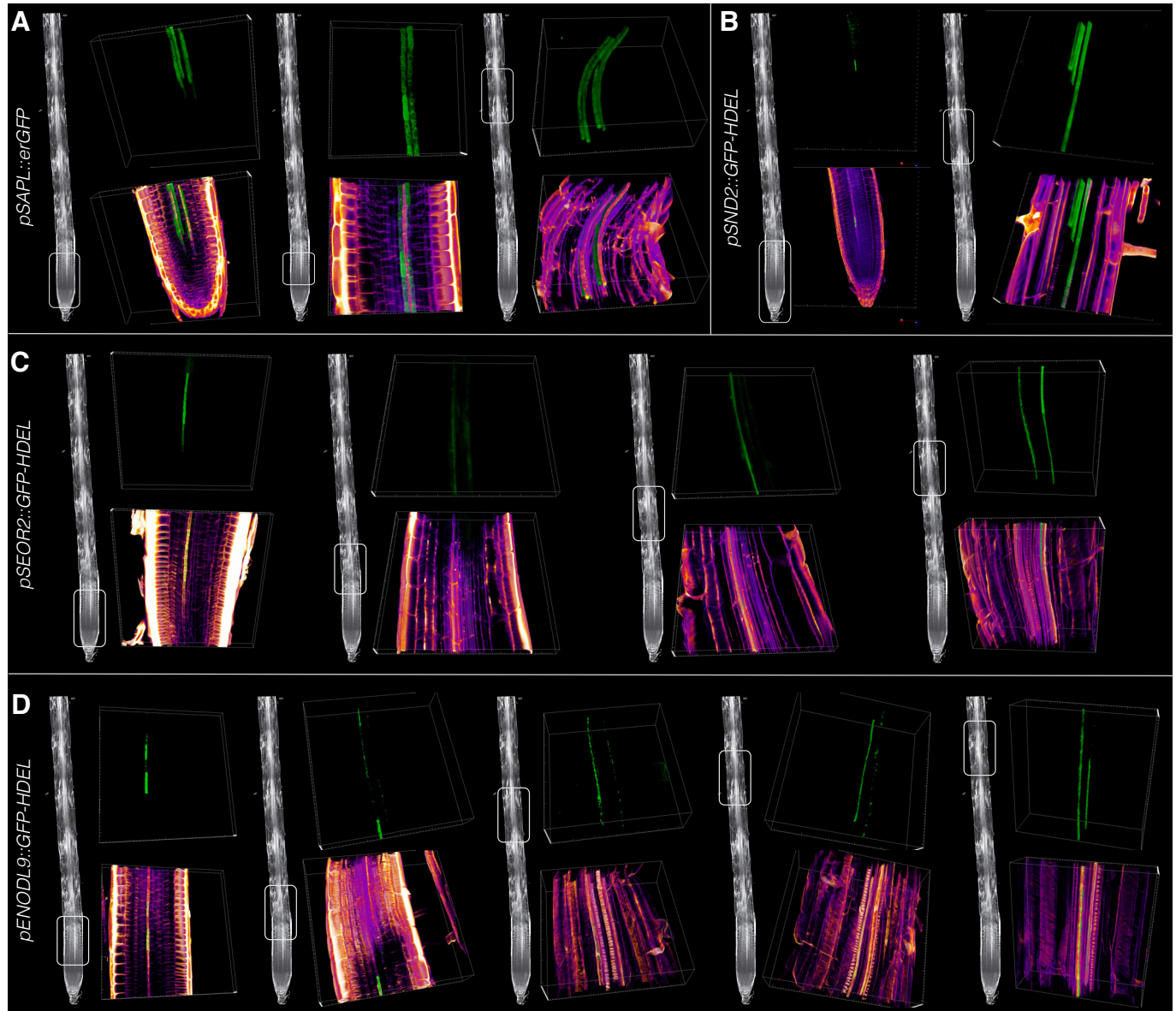


**Fig. 3. Reporter genes for phloem specification and differentiation I.** (A-D) 3D renderings of confocal image stacks, focused on the vasculature of 7-day-old CCFW-stained roots that express the indicated reporter genes (green fluorescence). Left overview panels (generic wildtype root) indicate the approximate positions of the magnified images in the right panels. Bottom panels: CCFW-GFP fluorescence composite images; top panels: GFP fluorescence only. Note that for better visibility of details, images are not always to the same scale.

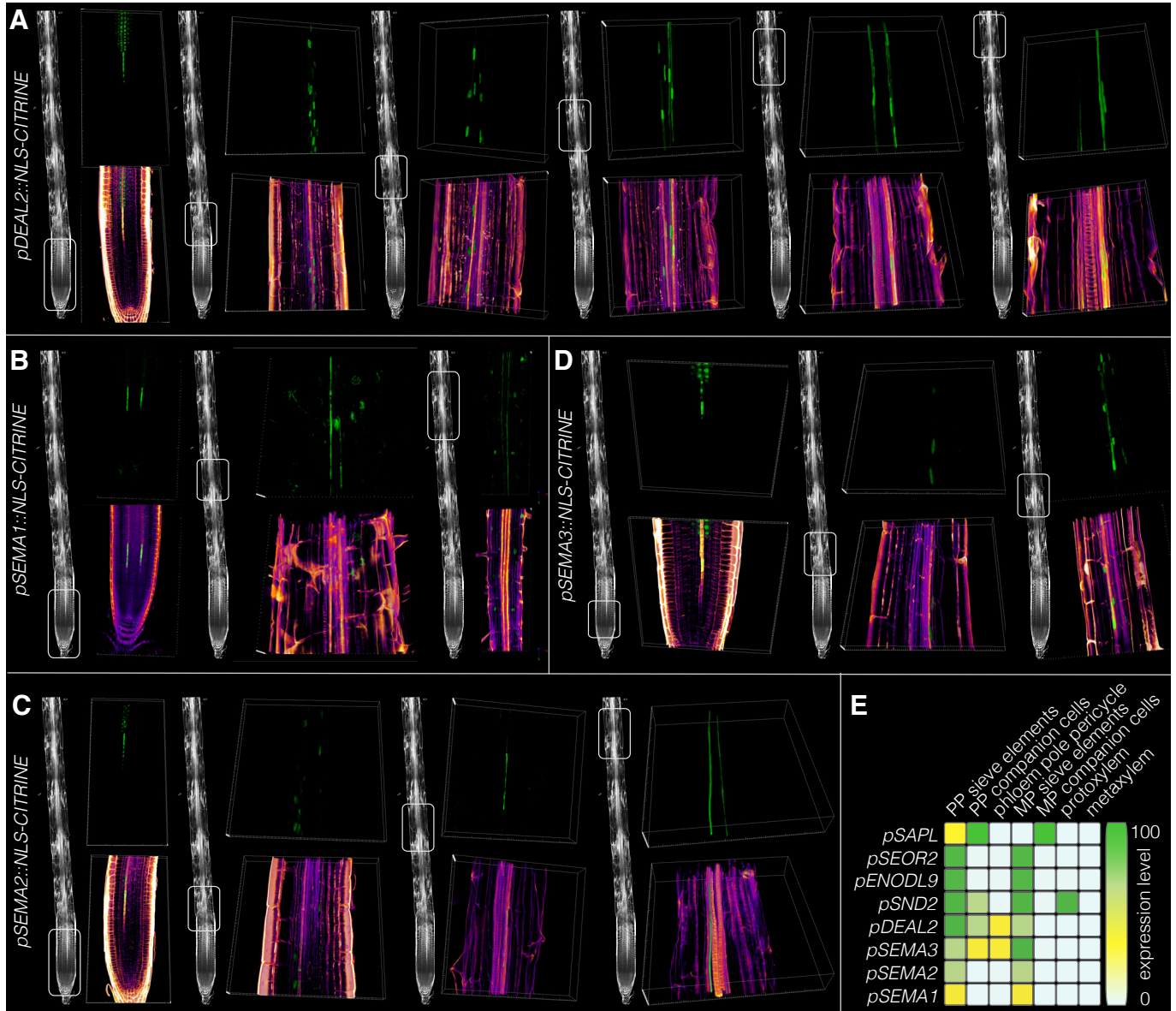


**Fig. 4. Reporter genes for phloem specification and differentiation II.** (A-D) 3D renderings of confocal image stacks, focused on the vasculature of 7-day-old CCFW-stained roots that express the indicated reporter genes (green fluorescence). Left overview panels (generic wildtype root) indicate the approximate positions of the magnified images in the right panels. Bottom panels: CCFW-GFP fluorescence composite images; top panels: GFP fluorescence only. (E) Schematic summary of the tissue-specific expression patterns for the reporter genes shown in figures 3 and 4.



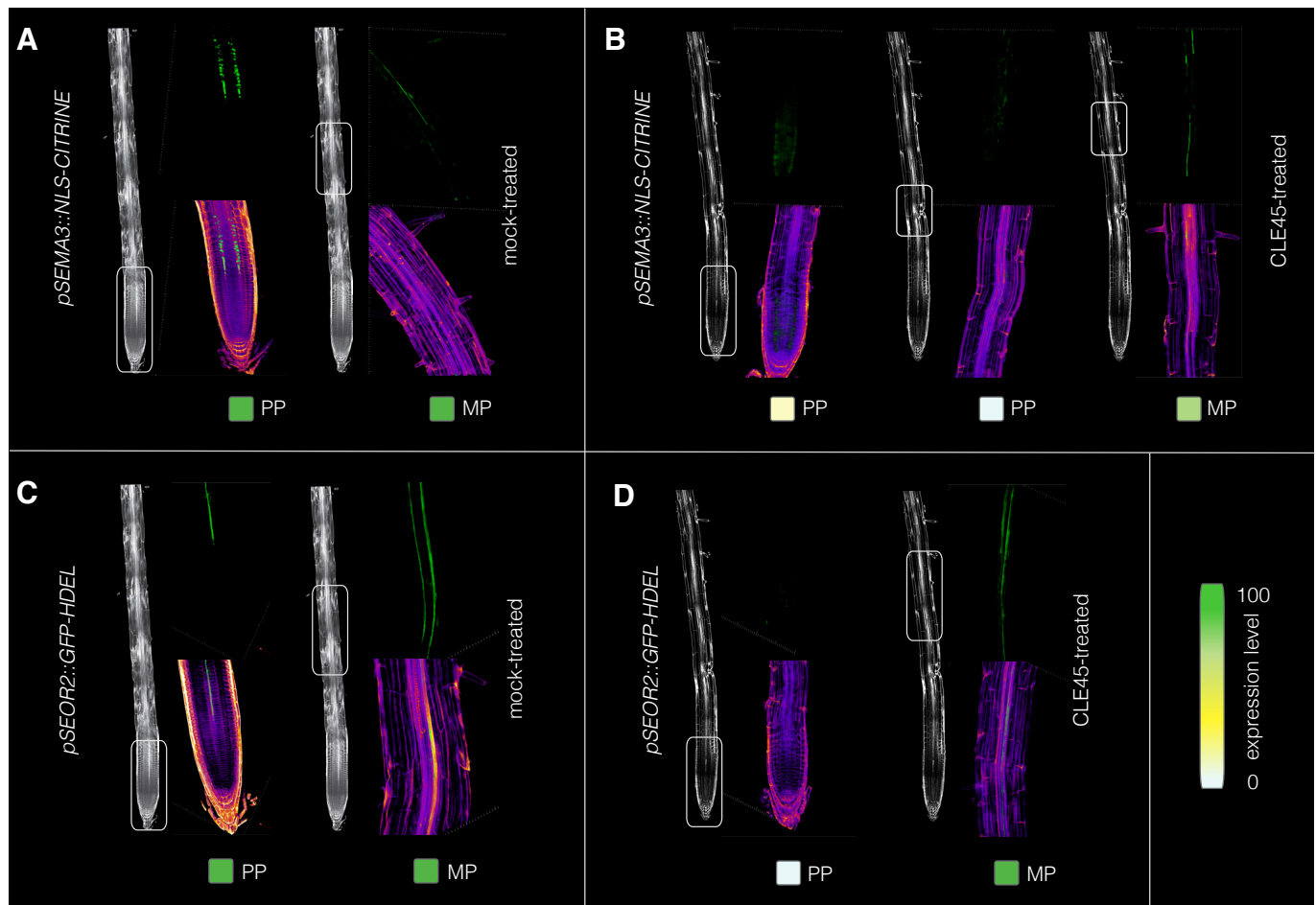


**Fig. 5. MPSE reporter genes do not respond to CLE45-treatment.** (A-D) 3D renderings of confocal image stacks, focused on the vasculature of 7-day-old CCFW-stained roots that express the indicated reporter genes (green fluorescence). Left overview panels (generic wildtype root, treated with mock or CLE45) indicate the approximate positions of the magnified images in the right panels. Bottom panels: CCFW-GFP fluorescence composite images; top panels: GFP fluorescence only. Roots were either grown on mock (A,C) or 15 nM CLE45 peptide (B,D).

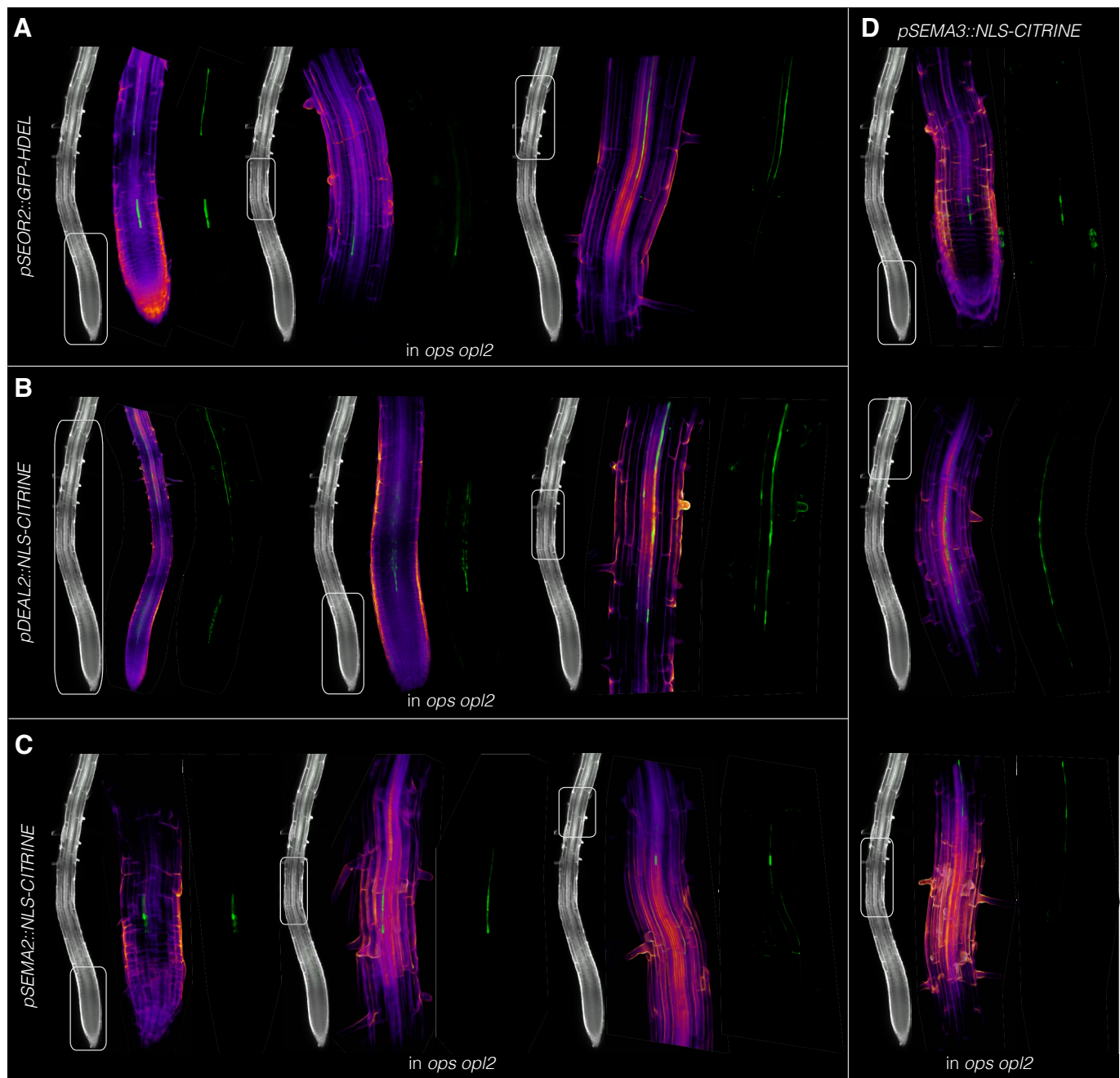


**Fig. 6. Phloem reporter gene expression in *ops opl2* double mutants I.** (A-D) 3D renderings of confocal image stacks, focused on the vasculature of 7-day-old CCFW-stained roots that express the indicated reporter genes (green fluorescence) in *ops opl2* double mutant background. Left overview panels (generic *ops opl2* root) indicate the approximate positions of the magnified images in the right panels. Center panels: CCFW-GFP fluorescence composite images; right panels: GFP fluorescence only. Note that for better viewing of details, images are not always to the same scale.

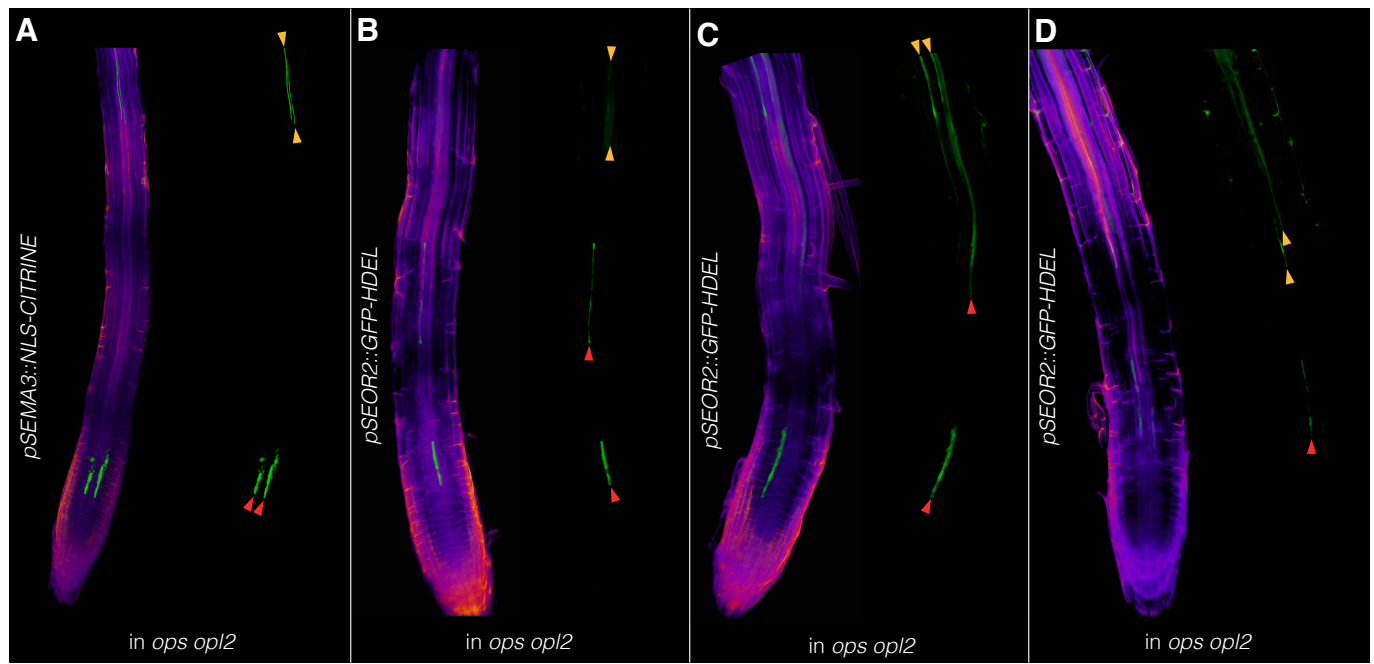


**Fig. 7. Phloem reporter gene expression in *ops opl2* double mutants II.** (A-D) 3D renderings of confocal image stacks, focused on the vasculature of 7-day-old CCFW-stained roots that express the indicated reporter genes (green fluorescence) in *ops opl2* double mutant background. Left panels: CCFW-GFP fluorescence composite images; right panels: GFP fluorescence only. PPSE or MPSE cell files expressing molecular markers are pointed out by red or orange arrowheads, respectively.

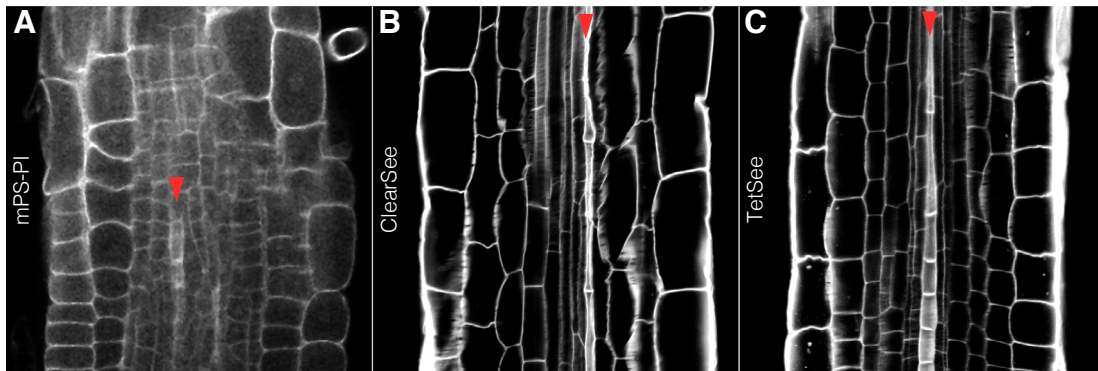


**Fig. S1. Imaging of elongating root cells using different fixation protocols.** (A-C) Confocal microscopy, optical sections of 7-day-old CCFW-stained root meristems (white fluorescence) fixed with different protocols as indicated. Red arrowheads point out elongating PPSEs.

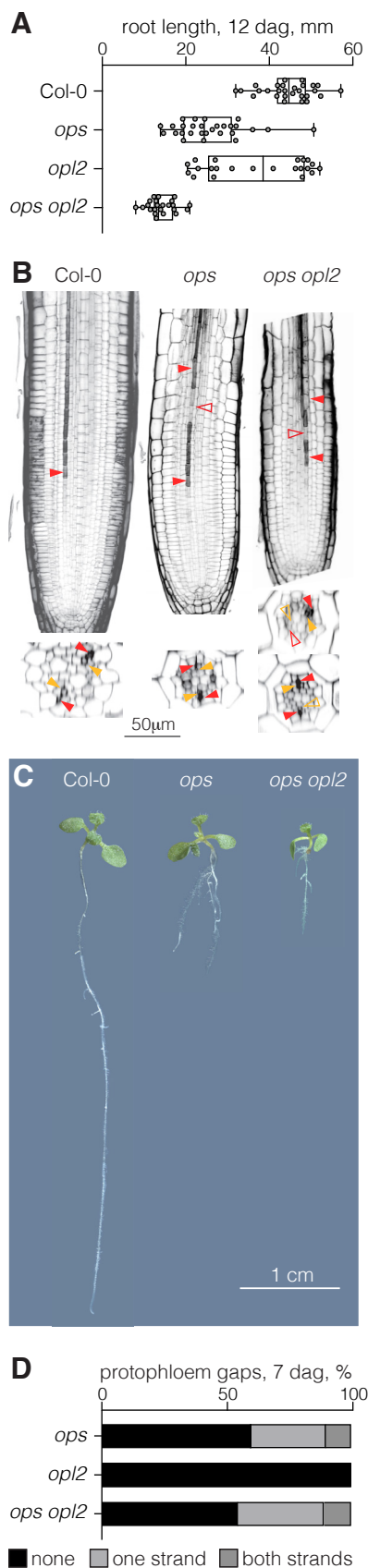


**Fig. S2. Root phenotypes of *ops opl2* double mutants.** (A) Primary root length of 12-day-old seedlings of indicated genotypes. Box plots display 2nd and 3rd quartiles and the median, bars indicate maximum and minimum. (B) Confocal microscopy, longitudinal and horizontal optical cross sections of 7-day-old CCFW-stained root meristems (black fluorescence). Full red arrowheads point out normally differentiating PPSEs, open red arrowheads point out cells in the PPSE file that fail to differentiate (“gap cells”). (C) Images of 12-day-old seedlings of the indicated genotypes. (D) Frequency of PPSE cell files with gap cells in root meristems of the indicated genotypes (n=20-30).

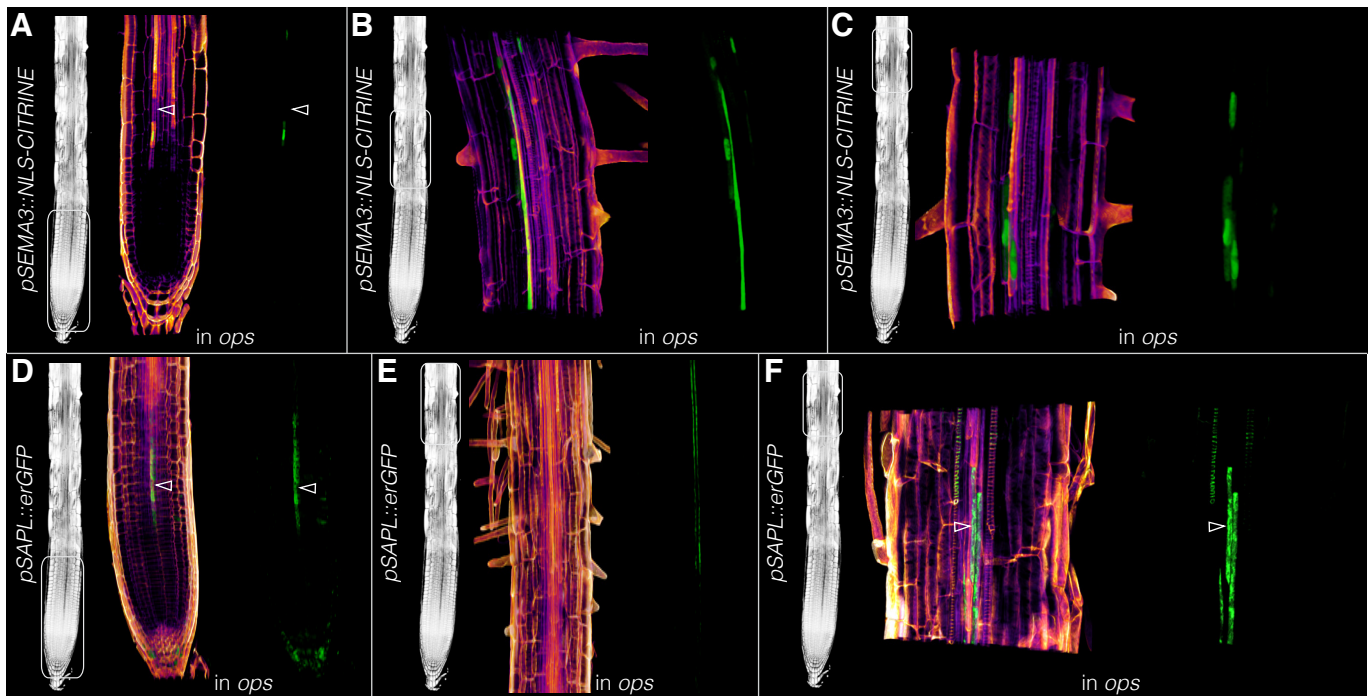


**Fig. S3. Phloem reporter gene expression in *ops* single mutants.** (A-F) 3D renderings of confocal image stacks, focused on the vasculature of 7-day-old CCFW-stained roots that express the indicated reporter genes (green fluorescence) in *ops* single mutant background. Left overview panels (generic *ops* root) indicate the approximate positions of the magnified images in the right panels. Center panels: CCFW-GFP fluorescence composite images; top panels: GFP fluorescence only. Note that for better viewing of details, images are not always to the same scale. Open arrowheads in (A), (D) and (F) point out cells in the PPSE file that fail to differentiate ("gap cells").

**Table S1**

5' to 3' oligonucleotide sequences

oligos with attB4/1r extensions				
oligo_name	sequence	gene	name	target
pAT2G44000_attB4_1F	ggggacaactttgtatagaaaagtgtGCTTGTATGCTGCTGGACA	AT2G44000	LEA hydroxylprolin	promoter
pAT2G44000_attB1r_1R	ggggactgctttttgtacaaactgtCATTCCCTCAGAGATTGTTT	AT2G44000		
pAT5G50120_attB4_1F	ggggacaactttgtatagaaaagtgtCGTGTTTCCCCACTTCTA	AT5G50120	WD40 Transducin-like	promoter
pAT5G50120_attB1r_1R	ggggactgctttttgtacaaactgtGGATTCTGAAATTGTATCATTTTTG	AT5G50120		
pAT2G35585_attB4_1F	ggggacaactttgtatagaaaagtgtGGTGACGATCGGAGGATA	AT2G35585	SEMA1	promoter
pAT2G35585_attB1r_1R	ggggactgctttttgtacaaactgtGAAATACCAACCATGATTGAA	AT2G35585		
pAT3G26350_attB4_1F	ggggacaactttgtatagaaaagtgtGATAGCGAAGCGAGTTACGG	AT3G26350	SEMA3	promoter
pAT3G26350_attB1r_1R	ggggactgctttttgtacaaactgtCATTAGATGAAGAAGTAAAAAGCA	AT3G26350		
pAT5G45320_attB4_1F	ggggacaactttgtatagaaaagtgtCTTCTGAAGCGCAGCTTCT	AT5G45320	LEA hydroxylprolin	promoter
pAT5G45320_attB1r_1R	ggggactgctttttgtacaaactgtACGAGAAGTCAATCTGGGCA	AT5G45320		
pAT3G63050_attB4_1F	ggggacaactttgtatagaaaagtgtTTCCGTGGAAGTGGTGC	AT3G63050	B-cell receptor associated 31 family	promoter
pAT3G63050_attB1r_1R	ggggactgctttttgtacaaactgtATCATTGTCTCTCTGCATCG	AT3G63050		
pAT1G61760_attB4_1F	ggggacaactttgtatagaaaagtgtTTAATTTTGTGGCCATT	AT1G61760	SEMA2	promoter
pAT1G61760_attB1r_1R	ggggactgctttttgtacaaactgtAGAATCGACCTGTGTGCA	AT1G61760		
pAT2G17260_attB4_1F	ggggacaactttgtatagaaaagtgtTTTCCGATTGATGATTTCC	AT2G17260	Glutamate receptor 2	promoter
pAT2G17260_attB1r_1R	ggggactgctttttgtacaaactgtCATGGACAACCCAGCAGTG	AT2G17260		
pAT2G14620_attB4_1F	ggggacaactttgtatagaaaagtgtTGCCTATGGCTGAAAAGTCC	AT2G14620	XTH10	promoter
pAT2G14620_attB1r_1R	ggggactgctttttgtacaaactgtCATTATTAAGATGTTGAGGTTGAG	AT2G14620		
pAT4G21310_attB4_1F	ggggacaactttgtatagaaaagtgtTGAGGGTGACCATCAAAACA	AT4G21310	DUF1218 domain protein	promoter
pAT4G21310_attB1r_1R	ggggactgctttttgtacaaactgtCCCTACATTCCTGCCATT	AT4G21310		
pAT2G37610_attB4_1F	ggggacaactttgtatagaaaagtgtGGAGGAGGAAGGAAGATTG	AT2G37610	SMR12	promoter
pAT2G37610_attB1r_1R	ggggactgctttttgtacaaactgtTACGTTTCCAATCTCCATGTG	AT2G37610		
pAT1G73040_attB4_1F	ggggacaactttgtatagaaaagtgtAATTAGGGATGCGTTGCTTG	AT1G73040	Mannose/lectin binding family protein	promoter
pAT1G73040_attB1r_1R	ggggactgctttttgtacaaactgtCATGAGTCGTCTGTGTTTT	AT1G73040		
pAT1G06490_attB4_1F	ggggacaactttgtatagaaaagtgtCGTTGACGCAGCTTATCAAGT	AT1G06490	Glucan synthase like 7	promoter
pAT1G06490_attB1r_1R	ggggactgctttttgtacaaactgtCATAATAGTGATCAATTTCAAATTC	AT1G06490		
pAT5G04890_attB4_1F	ggggacaactttgtatagaaaagtgtccagtttcaactccgttttg	AT5G04890	RTM2	promoter
pAT5G04890_attB1r_1R	ggggactgctttttgtacaaactgtCATtatttaattacttcttctctc	AT5G04890		
pAT3G49380_attB4_1F	ggggacaactttgtatagaaaagtgtTGATGAGAAATTTATCTGTTTTGGA	AT3G49380	IQD15	promoter
pAT3G49380_attB1r_1R	ggggactgctttttgtacaaactgtCAAGATCGATCAACCTCGTCT	AT3G49380		
oligos with attB1/2 extensions				
oligo_name	sequence	gene	name	target
pAT4G28500_attB1_1F	ggggacaagttgtacaaaaagcaggcttcgaccaccaatgaaaaca	AT4G28500	SND2	promoter
pAT4G28500_attB2_1R	ggggaccactttgtacaagaagctgggtCATgtttgtgtgtccctaagtt	AT4G28500		
pAT3G06172_attB1_1F	ggggacaagttgtacaaaaagcaggctcagctggagaacttacaatacaaa	AT3G06172	SEOR2	promoter
pAT3G06173_attB2_1R	ggggaccactttgtacaagaagctgggtTTGAAAGCGTTGGCCAT	AT3G06173		
pAT3G20570_attB1_1F	ggggacaagttgtacaaaaagcaggctTctcagattagttggcctttt	AT3G20570	ENODL9	promoter
pAT3G20570_attB2_1R	ggggaccactttgtacaagaagctgggtGTGTAGGAATAGAGTGGAGCTAGA	AT3G20570		